

Pathway-based Bayesian inference of drug–disease interactions†

Naruemon Pratanwanich and Pietro Lió*

Cite this: *Mol. BioSyst.*, 2014, **10**, 1538

Drug treatments often perturb the activities of certain pathways, sets of functionally related genes. Examining pathways/gene sets that are responsive to drug treatments instead of a simple list of regulated genes can advance our understanding about such cellular processes after perturbations. In general, pathways do not work in isolation and their connections can cause secondary effects. To address this, we present a new method to better identify pathway responsiveness to drug treatments and simultaneously to determine between-pathway interactions. Firstly, we developed a Bayesian matrix factorisation of gene expression data together with known gene–pathway memberships to identify pathways perturbed by drugs. Secondly, in order to determine the interactions between pathways, we implemented a Gaussian Markov Random Field (GMRF) under the matrix factorization framework. Assuming a Gaussian distribution of pathway responsiveness, we calculated the correlations between pathways. We applied the combination of the Bayesian factor model and the GMRF to analyse gene expression data of 1169 drugs with 236 known pathways, 66 of which were disease-related pathways. Our model yielded a significantly higher average precision than the existing methods for identifying pathway responsiveness to drugs that affected multiple pathways. This implies the advantage of the between-pathway interactions and confirms our assumption that pathways are not independent, an aspect that has been commonly overlooked in the existing methods. Additionally, we demonstrate four case studies illustrating that the between-pathway network enhances the performance of pathway identification and provides insights into disease comorbidity, drug repositioning, and tissue-specific comparative analysis of drug treatments.

Received 7th January 2014,
Accepted 9th March 2014

DOI: 10.1039/c4mb00014e

www.rsc.org/molecularbiosystems

1 Introduction

Cellular processes before and after drug treatments often result from the concerted interactions of certain sets of genes. Traditionally, microarray-based case–control studies provide the information about such mechanisms through a list of differentially expressed genes. It has currently become of great interest to analyse at the level of pathways/gene sets instead of individual genes. This is because firstly looking at the pathway/group level can reduce the complexity of the analysis due to the dimension reduction. Secondly, some of the important differences may not be detected in the simple gene list because of the dominating noise inherent to the microarray technology.¹ Finally, the gene-wise approach limits the scalability of comparative studies, since the gene list profiles may marginally overlap between two independent experiments despite being under the same biological conditions (*e.g.* drug treatments or disease states).¹ In contrast, the pathway-based approach can overcome

these limitations since pathways already embody functionally related genes, providing interpretable information with low dimensionality. This also allows a certain variation of genes that are differently expressed under the same biological conditions.

Notably, connections between genes may trigger unexpected effects. On one hand, the interactions can cause negative outcomes such as comorbidity, the presence of one or more diseases co-occurring with the primary disease. In particular, Goh *et al.* have assumed that diseases could comorbid with each other through overlapping disease-causing genes, as represented by the human disease network (HDN).² On the other hand, the links between genes can also bring medical benefits that enable poly-pharmacology and drug repositioning. For example, the network of drug targets and disease-related genes can help determine the new potential indications of the existing drugs.³ As connections exist not only within a pathway but also across different pathways, the network of pathway interactions still remains to be established.

To better understand cellular processes in case–control settings, we aim to source microarray data in an efficient manner. Firstly, we have developed a Bayesian matrix factorisation of gene expression data and taken advantage of known

University of Cambridge, JJ Thomson Avenue, CB3 0FD, UK.

E-mail: np394@cam.ac.uk, pl219@cam.ac.uk

† Electronic supplementary information (ESI) available. See DOI: 10.1039/c4mb00014e



gene–pathway memberships to identify pathway responsiveness. Secondly, we have augmented the Bayesian factor model with a GMRF to determine the interactions between pathways. Assuming the GMRF prior of pathway responsiveness, we used the precision (inverse co-variance) matrix of a Gaussian distribution to model the correlations between pathways.⁴ In this study, we applied the combination of the Bayesian factor models and the GMRF to analyse gene expression data of drug treatments.

GMRF models have been widely developed to learn spatial interactions.^{5,6} Recently, they have been used for the analysis of genomic data to identify causal or marker genes and simultaneously to reconstruct between-gene interactions.^{7,8} To the best of our knowledge, this is the first effort to apply the GMRF model to reconstruct the network of between-pathway interactions.

As for responsive pathway identification, many studies extracted responsive pathways by leveraging gene expression data for the network of gene interactions, regardless of the prior knowledge about gene–pathway memberships.^{9–11} These results would leave a burden of expertise for interpretation. Ma and Zhao developed a Bayesian factor model for identifying pathway responsiveness, called FacPad, which utilises the prior knowledge of gene–pathway memberships.¹² Similarly, a well-known method, Gene Set Enrichment Analysis (GSEA), determines whether a pre-defined pathway is enriched in a given gene expression profile using statistical scores.¹ However, both have assumed that individual pathways are independent, which limits to reflect the realistic molecular activities. We have overcome this limitation by implementing a GMRF to model the dependencies between pathways. This GMRF extension improves the performance of responsive pathway identification.

Modeling pathway dependencies, which are regarded as latent structures, is challenging because they cannot be observed directly from the data. Although the issue of dependency structure in latent space has been solved,^{13,14} the literature concerning between-pathway relationships is still limited. Luo *et al.* connected two pathways through the overlapping perturbed member genes in time series gene expression data,¹⁵ but only a few pathways were analysed. Recently, Pang and Zhao developed a large-scale pathway clustering method based on the inferred distances where each pathway was used as a classification tree to predict classes of phenotypes from gene expression data, and two pathways were considered similar if they predicted the same class of phenotypes.¹⁶ However, while they predicted the between-pathway relations deterministically after the classification tasks, we probabilistically modeled such interactions concurrently with the pathway responsiveness identification task. Due to the simultaneous tasking in our model, not only can the results from the identification part reflect pathway dependency behaviours, but also the pathway interactions help improve the accuracy to identify pathway responsiveness to drug treatments.

2 Data

Our model requires two types of data inputs – differential gene expression data and known gene–pathway associations informing gene memberships in each pathway. We utilised gene expression data of drug treatments from the human breast epithelial

adenocarcinoma cell line (MCF7) provided by CMap (build 02),^{17,18} and exploited the prior knowledge of gene–pathway memberships from Kyoto Encyclopedia of the Genes and Genomes (KEGG) database.¹⁹ After pre-processing (see the ESI† for more details), 3041 genes, 1169 drugs, and 236 known pathways (90% of the total KEGG pathways), 66 of which were disease pathways, remained in our analysis. We applied our model to another gene expression data set of the epithelial cell line of human prostate adenocarcinoma (PC3) from CMap^{17,18} for tissue comparative analysis as discussed in the final case study.

3 Results and discussion

Identifying pathway responsiveness under any biological conditions (*e.g.* drug treatments and disease conditions) can be accomplished using a Bayesian factor model.¹² We modeled pathways as latent variables, of which gene members were pre-defined.¹² More importantly, we implemented a GMRF prior in order to capture the network structure of interactions between pathways.

Given the differential gene expression data and the prior knowledge of gene–pathway memberships, we inferred the following: (1) pathway responsiveness specific to each biological condition and (2) interactions between pathways (Fig. 1). The novelty of this study lies in the latter, which contributed the network of between-pathway interactions.

In the next section, we show the results of model verification and validation including comparison with the other existing models, followed by four case studies as to how this inferred pathway network helps us to understand the underlying mechanisms among drugs and diseases.

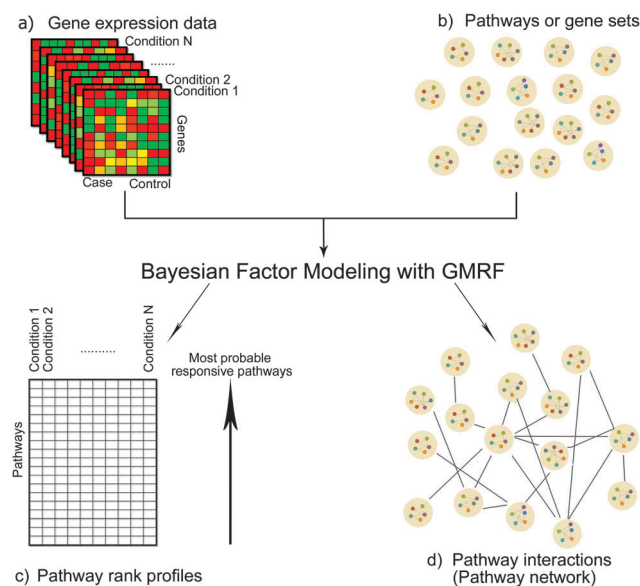


Fig. 1 Diagram of our methodology. The inputs are (a) differential gene expression data under conditions of interest (*e.g.* drug treatments or disease states) and (b) pathways/gene sets, in which individual gene members are defined. We developed a Bayesian factor model with GMRF to infer (c) pathway rank profiles specific to each condition and (d) the interactions between pathways, which can be viewed as a pathway network.



3.1 Model verification with simulation studies

To verify our model, we synthesised different gene expression data sets of 3000 genes and 2000 drugs from a Gaussian distribution with respect to a random but known underlying network of between-pathway interactions that varied over 10, 20, 50, and 80 pathways. Next, we assigned some pathways to each drug as its responsive pathways. Finally, we assessed for our model how many original between-pathway interactions were recovered and how many responsive pathways were identified correctly. We used recall and precision metrics to evaluate the performance of our inference on the pathway network and accuracy metric for the assessment of pathway identification.

Fig. 2 shows the overall performance of our model on the different synthetic data sets. Although the performance was dropping when the number of pathways was increasing, it was no less than 80% (Fig. 2a). On the other hand, an increase in density slightly affected the model performance (Fig. 2b). We also conducted the robustness analysis of noise tolerance. Here, noise can be originated from both inputs, the gene expression data and the information of gene–pathway memberships. However, we tested our model only with the noise caused by the latter case because we already incorporated the noise model from the first case. Our model proved its robustness up to 30% of noise (Fig. 2c).

3.2 Model validation and comparative studies

To validate, we applied our model to analyse gene expression data of drug treatments from CMap and exploited the prior information of gene–pathway memberships from KEGG. We then evaluated two outputs: the pathway rank profiles responsive

to drug treatments and the network of between-pathway interactions.

3.2.1 Analysis of the inferred pathway responsiveness to drug treatments. Pathways that were perturbed by chemical exposures were documented in the Comparative Toxicogenomics Database (CTD).²⁰ The significance of the enrichment for each pathway was computed by a hypergeometric distribution and adjusted by a Bonferroni approach for multiple hypothesis testing. We validated the inferred pathways responsive to drug treatments with the CTD data as of June 4th 2013. After post-processing, 500 drugs, 193 pathways, and 14 502 chemical–pathway associations were left for the validation.

In each drug d , we ranked all pathways according to their inferred responsiveness values. The ranked list of pathways is called a pathway rank profile where pathways at the upper ranks are more likely to be responsive to drug d . Fig. 3 demonstrates the frequency of pathways that were documented in CTD in each rank of the inferred pathway rank profiles. We found that 210 drugs were identified at the first rank, which was 1.5–2.6 times higher than random expectation. Furthermore, our method identified the perturbed pathways at the upper ranks than those inferred by FacPad and GSEA ($p < 0.0001$).

Using the validation set from CTD, we also calculated the average precision (AP)²¹ over the recall ranged from 0 to 1, as shown in eqn (1) for each drug d :

$$AP = \frac{\sum_{r=1}^R (P_r \times l_r)}{N}; P_r = \frac{n_r}{r} \quad (1)$$

where l_r is 1 when the pathway at rank r was documented in CTD and 0 otherwise, n_r is the number of pathways validated by

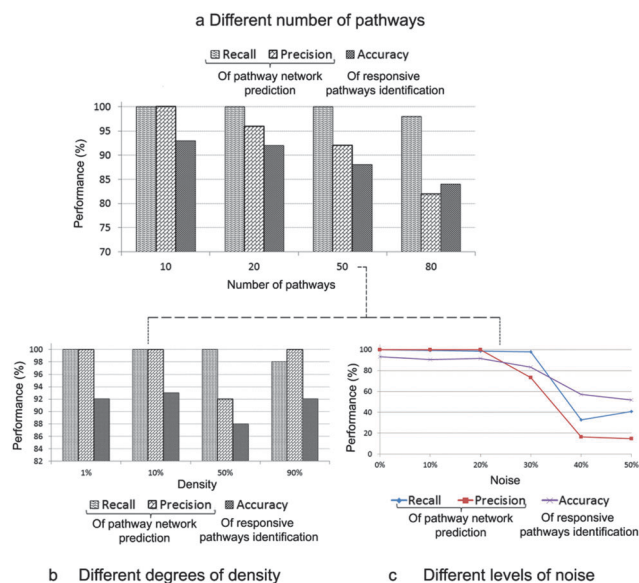


Fig. 2 Performance of our model on the synthetic data sets varied by (a) the number of pathways, (b) degree of density, (c) and the noise level. We found that by increasing the number of pathways, model performance decreased by a negligible amount, whereas varying the degree of density only slightly affected the model performance. Additionally, by sensitising noise levels in the data up to the 30% level, the model results remained robust, but began to fail from 40% onwards.

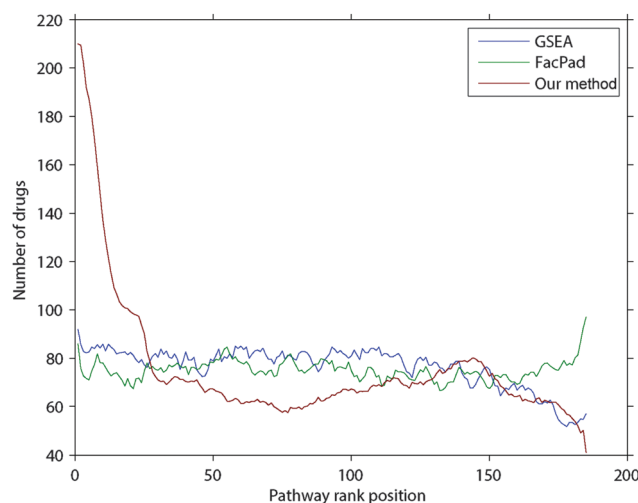


Fig. 3 Performance of three methods for identifying pathway responsiveness. We first created pathway rank profiles, each of which was specific to a drug and pathways in the upper ranks are more likely to have high responsiveness. Out of 500 drugs in the validation set, the number of pathways that were documented by CTD as true responsive pathways in the rank profiles of each method is shown in the y-axis across the pathway rank positions in the x-axis. In the upper ranks, our model recovered more true responsive pathways than the other methods.



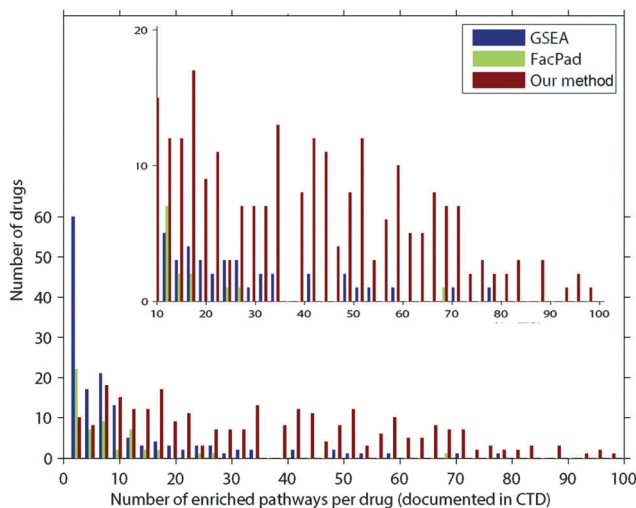


Fig. 4 Comparison of the average precision values for evaluating each pathway rank profile from our model, FacPad, and GSEA. We calculated the average precision (eqn (1)) for each profile and compared this metric among the methods. Out of 500 drugs in the validation set, the number of pathway rank profiles with the highest average precision in each model is demonstrated in the y-axis. We classified drugs according to the number of enriched pathways per drug as documented in CTD shown in the x-axis. We found that our model outperformed the others for identifying responsive pathways in the case of drugs that had an effect on more than 10 pathways. These results are illustrated in the refined scale with a y-axis ranging from 0 to 20 in the inset plot.

CTD from the top r ranks, thus P_r is the precision at the rank r th, N is the total number of enriched pathways defined by CTD, and R is the total number of pathways. The number of drugs with the highest AP of each model was plotted across the number of enriched pathways per drug as documented in CTD (Fig. 4). As shown, FacPad and GSEA were excellent for identifying pathways responsive to the drugs that perturbed not more than ten pathways. However, when the number of perturbed pathways per drug increased, our model yielded the higher AP ($p < 0.0001$).

3.2.2 Analysis of the inferred between-pathway interactions.

In this study, we inferred the interactions between pathways solely from the presence of their co-occurrence in the observed data. As a result, not only were the interactions of any pathway pairs that shared genes together likely to be drawn, but any other pathway pair without overlapping genes could be also inferred if they co-occurred in the observed gene expression data.

Theoretically, there are many factors why pathways interact with each other, one of which is the overlapping of their gene members. Thus, we used the number of the overlapping genes between two pathways from the curated KEGG database to quantify the validity of our results. We first ranked the pathway interactions according to their correlations derived from our approach (eqn (5)). We then applied the cumulative gain (CG),²² to determine whether the inferred interactions at the upper ranks were more likely to imply true interactions. Here, the number of overlapping genes indicated the possibility of true interactions between pathways. For each rank r , we calculated the ratio between the CG of our model and that of the random

expectation, called fold enrichment of cumulative gain (FE_CG_{*r*}) as in eqn (2):

$$\text{FE_CG}_r = \frac{\text{Model_CG}_r}{\text{Random_CG}_r} = \frac{n_r}{N \times r/R} \quad (2)$$

where Model_CG_{*r*} stands for the cumulative gain at rank r of our model, where n_r is the cumulative number of overlapping genes at rank r , and R is the total number of rank entries. Random_CG_{*r*} stands for the expected CG value by chance. Thus, FE_CG_{*r*} indicates how many times that the interactions inferred at the top- r rank are likely to be true interactions compared to those occurring by chance.

In addition, we calculated the significance of each pathway interaction in terms of perturbed member genes using a hypergeometric distribution¹⁵ (see the ESI†). Here, a perturbed gene was a gene with the absolute fold change deviated from the mean of all genes by more than one standard deviation. Let N , n , and x be the number of all perturbed genes under given conditions, in either of a pathway pair, or in both pathways respectively. The significance is the probability of at least X genes that are perturbed in both pathways, which follows the hypergeometric distribution¹⁵ as shown in eqn (3):

$$\text{Prob}(x \geq X) = \sum_{k=X}^{\min(n_1, n_2)} \frac{\binom{n_1}{k} \binom{N-n_1}{n_2-k}}{\binom{N}{n_2}} \quad (3)$$

After ranking the between-pathway interactions according to their correlation values (eqn (5)), we found that the top 500 interactions had high possibilities to be true interactions, approximately 2–6.5 times as much as expected by chance (Fig. 5a). Each of them had the correlation ranging from 0.05 to 0.5, while approximately 10 000 interactions stayed unconnected with zero values (see Methodology). Fig. 5b also shows that these interactions significantly contained more overlapping genes than the rest ($p < 0.001$).

However, we also modeled the interactions between pathways that did not share any genes. Fig. 6 compares the networks of the top 500 pathway interactions resulting from two methods. The first network of pathway interactions derived from our Bayesian factor model with GMRF (Fig. 6a). For the second network, two pathways were linked if they shared perturbed member genes¹⁵ and their interaction strength was proportional to the number of their overlapping genes (Fig. 6b). We mapped all 236 pathways into 22 classes based on the definition by KEGG with different colours. Fig. 6a contains 67% of inter pathway-class interactions while 42% in Fig. 6b. The high percentage of inter pathway-class interactions resulted from our model may imply the complex relationships beyond gene connections. For example, we uncovered the links between cancer and metabolism (Fig. 6b). According to the recent study,²³ metabolism first generates oxygen radicals which contribute to loss of tumor suppressors and finally lead to cancer. These cancer cells will in turn rewire back to metabolic pathways for cell growth and survival. We also rediscovered the interactions between cancer pathways and those of infectious diseases caused by viral,²⁴ bacterial,^{25,26} and parasitic²⁶ agents



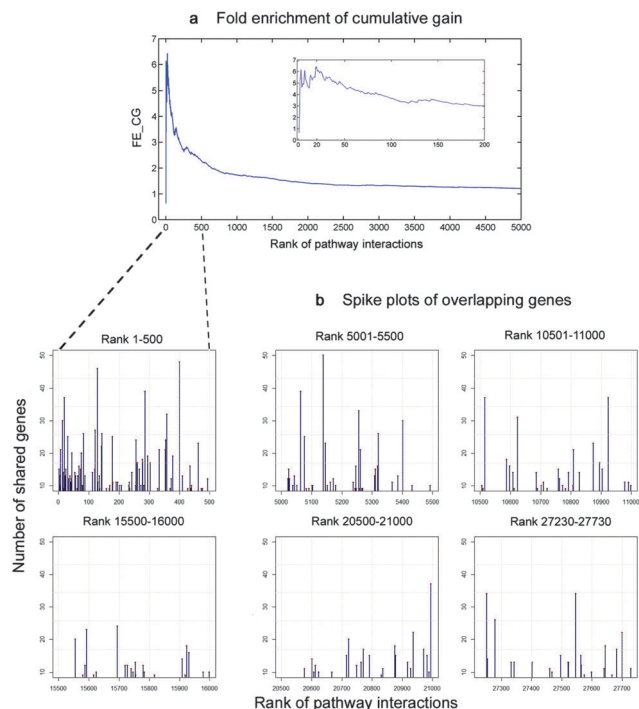


Fig. 5 Relation of our inferred pathway interactions and the number of overlapping genes. We defined true positives as the interactions of pathways that had genes in common. To validate, we ranked the pathway interactions by their correlations as calculated with our method in a descending order. We then counted the number of genes shared by any two pathways for every interaction. Next, we calculated the cumulative true positives weighted by the number of overlapping genes in each rank, also known as cumulative gain (CG),²² and compared this metric against random expected values. (a) Fold enrichment of cumulative gain (FE_CG) as calculated in eqn (2), which is the ratio between the CG of our model compared to random expectation,¹² reached the peak of (6.5 fold) at the upper ranks (20th). Out of 27730 possible interactions, the top 500 interactions inferred by our model were likely to share genes approximately 2–6.5 fold compared to the random expectation. (b) Number of overlapping genes of each interaction in six intervals, each of which equally spans to 500 rank positions. As shown, the density of spikes at the first 500-rank interval was at the maximum then it continually declined, and reached the minimum at the lower end of the ranks.

(Fig. 6b), while the other model reconstructed only the links with viral agents.

3.3 Applications of the pathway network

Case study 1: disease comorbidity through pathway-based interactions. Recently, comorbidity has been studied through different networks, where nodes represent diseases and edges represent the overlapping of mutated genes,² protein complexes,²⁷ metabolic reactions,²⁸ or pathways²⁹ between diseases. However, these networks are insufficient in case two diseases are linked by the concerted interactions of multiple pathways. Utilising our inferred pathway network can overcome this limitation, as nodes in our network can represent both disease and non-disease pathways.

In this case study, we explored a sub-network of the top 500 interactions, which contained the largest hub namely the hepatitis B pathway. We found that infectious diseases, especially hepatitis B

and C, connected with more than half of cancer types in our study (Fig. 7a). This finding agrees with the statistics from a survey of Cancer Research UK in 2008, showing that hepatitis B and C viruses are the third most attributable risk to cancers only after human papillomavirus and helicobacter pylori, which were not included in our study. Additionally, the inferred pathway network suggest that NF- κ B, followed by FC ϵ RI and GnRH signaling pathways be the main contributions underlying the comorbidity among infectious diseases and cancers.

Particularly, we can make a hypothesis that hepatitis B may comorbid with thyroid cancer through the mechanisms of FC ϵ RI and NF- κ B signaling pathways. The processes may begin with the increased level of serum Immunoglobulin E (IgE) in hepatitis B patients³⁰ that theoretically activates FC ϵ RI receptors as described in KEGG (inferred corr = 0.14, rank 33th, overlapping perturbed genes with $p < 0.0001$ from a hypergeometric test). We then confirmed the inferred interaction between NF- κ B and FC ϵ RI (inferred corr = 0.23, rank 10th, overlapping perturbed genes with $p < 0.005$) by the literature. Klemm and Ruland reported that the inflammatory signals in mast cells could be transmitted between these pathways through the following events: the activation of the receptor-associated tyrosine kinases upon Fc ϵ RI ligation, the activation of PKC isoforms and the protein complex of Bcl10/Malt1, the degradation of I κ B- α , and finally the activation of NF- κ B³¹ (Fig. 7b). Moreover, we rediscovered the association of the NF- κ B signaling pathway and the thyroid cancer pathway (corr = 0.10, rank 64th) even though they had no overlapping genes. Several studies have claimed that the activation of NF- κ B blocks the PRAR γ tumor suppressor, promoting thyroid carcinogenesis.^{32,33} As the relevance of NF- κ B and FC ϵ RI signaling pathways as well as the high prevalence of thyroid cancer in hepatitis patients³⁴ have recently been reported,^{35,36} our hypothesis that cancers may comorbid with infectious diseases through these inflammatory signaling pathways should be further studied.

Case study 2: enhancement of pathway responsiveness identification. In a pathway rank profile, pathways that have higher responsiveness are located at the upper ranks. Fig. 8 demonstrates examples of drugs, each of which targets two neighboring pathways in the sub network of Fig. 7a. Thanks to the guidance of the pathway network that we inferred concurrently with the pathway identification task, our method identified both pathways at the upper ranks. In contrast, FacPad¹² and GSEA¹ identified one at the upper rank, but left the other far behind near the bottom. These representatives prove the advantage of the pathway network for identifying pathway responsiveness.

Case study 3: drug repositioning via pathway-based inter-links. Given our inferred pathway network including disease-related pathways, we are able to discover a new potential indication of the existing drugs, known as drug repositioning. Unlike the existing similarity-based methods,^{37,38} the inferred pathway network provides the underlying pathways as inter-links between the repositioned drugs and their new targeted disease.

For example, we repositioned Verapamil, which has been currently used for the treatment of angina and hypertension, to the new indication for colorectal cancer. As documented in



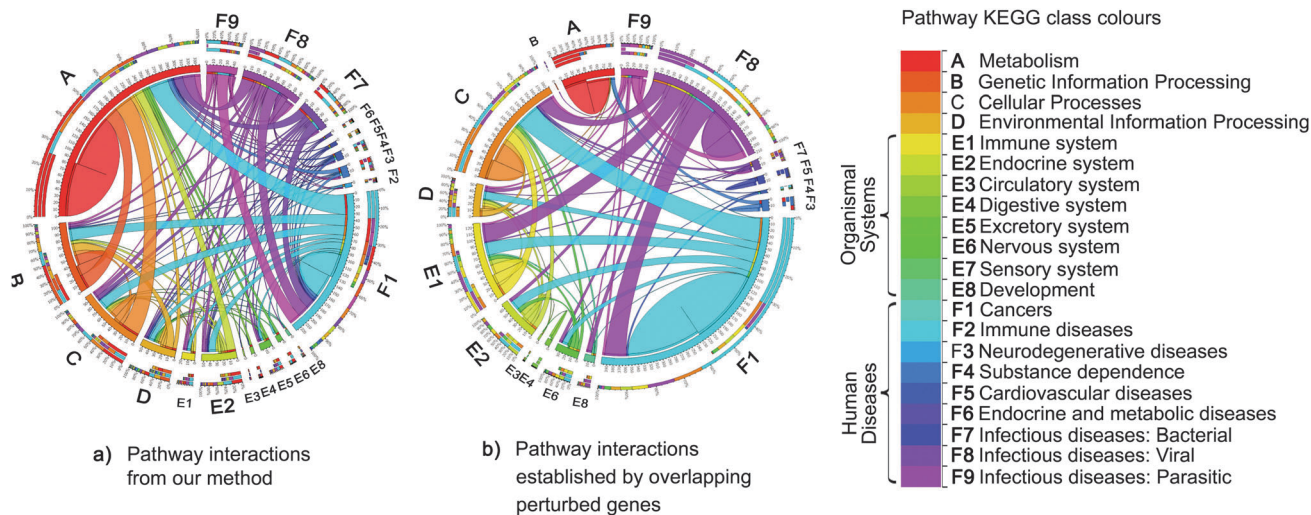


Fig. 6 Comparisons of pathway interactions. The colour of each pathway maps to each class of pathway defined by KEGG. The edge size is proportional to the number of interactions from one pathway class to another. Each interaction is established by two methods. (a) Firstly, pathway interactions resulted from our Bayesian factor model with GMRF. (b) Secondly, two pathways were linked if they shared perturbed member genes.¹⁵ Of top 500 interactions, our approach yielded more interactions across different classes of pathways, nearly double the number of interactions relative to the second method (b), which discovered more intra pathway-class interactions. For instance, the relationships between cancers and metabolism pathways²³ rediscovered by our method were absent from the second method (b). The second method limits to capture the interactions between pathways without overlapping genes. In contrast, our method can model pathway interactions according to both overlapping genes and the co-occurrence of pathways observed in the gene expression data.

CTD and inferred by our method, this compound targeted the GnRH signaling pathway, which linked colorectal cancer in the inferred pathway network as shown in Fig. 8 (corr = 0.06, rank 261th, shared perturbed genes with $p < 0.001$). This suggests the new indication of Verapamil to recover the disease state of colorectal cancer. Our hypothesis is in line with the independent studies claiming that Verapamil could suppress the release of GnRH hormone³⁹ which is over-expressed in colorectal cancer.⁴⁰ More recently, this drug repositioning has been confirmed by a clinical study concluding that the use of Verapamil with chemotherapy can improve clinical efficacy in metastatic colorectal patients.⁴¹

Upon the integration of the pathway network and responsive pathway identification from our method, we can provide informative hypotheses of not only the directions to reposition drugs but also the underlying pathways to explain the new drug-disease mechanisms.

Case study 4: tissue comparative analysis. Since whether or not genes are active partly depends on tissue types, the between-pathway relationships can be different from tissue to tissue. Thus, we applied the model to two different tissue-specific data sets from CMap, the breast cancer cell line (MCF7) and the prostate cell line (PC3). Although some pathway associations were inferred at the upper ranks in both tissues, others were different. For example, the inferred interaction of the FcεRI signaling pathway and the NF-κB signaling pathway fell from the rank 10th in MCF7 to 11 765th in PC3. There exist evidences that both pathways are linked in mast cells;³¹ however, the study concerning the issue of tissue types is still limited. Generally, FcεRI plays a central role in the initiation and control of atopic allergic inflammation⁴² and NF-κB

involves in many cancers.⁴³ Thus, the existence of the interaction between these two pathways may account for the role of allergic disorders differs between the development of cancer cells in breast and prostate tissues.⁴⁴ Such a difference in between-pathway interactions in different tissue types can improve our understanding of disease mechanisms, leading to the advance in tissue-specific therapies.^{45,46}

4 Methodology

4.1 Notation

In this paper, we represent a matrix, a vector, and a scalar with a bold capital letter, a bold lowercase letter, and an italic lowercase letter respectively. Moreover, we use double brackets to represent a matrix and its elements such as $\mathbf{X} = [[x_{ij}]]$, indicating that the matrix \mathbf{X} consists of the scalar elements x_{ij} where i and j denote a row index and a column index respectively.

4.2 Method overview

In this study, we have performed the analysis of the differential gene expression data of G genes under D conditions. Our goal is to identify responsive pathways for each condition and simultaneously to uncover between-pathway relationships. To begin with, we assume that the differential gene expression data arise from the effects of perturbed genes being members of the pathways responsive to each condition *e.g.* a drug or a disease. This concept can be implemented by a matrix factorisation,¹² where the observed differential gene expression data matrix $\mathbf{X} \in \mathbb{R}^{G \times D}$ is decomposed into two matrices: $\mathbf{X} \sim \mathbf{BS}$. The first matrix $\mathbf{B} \in \mathbb{R}^{G \times P}$ denotes the strength of gene membership in



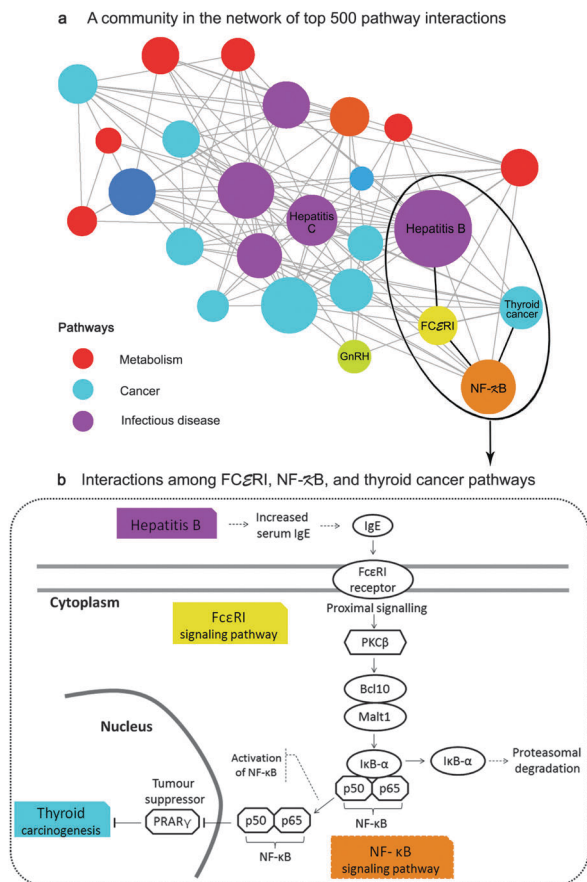


Fig. 7 Application of the pathway network for disease mechanisms and comorbidity (case study 1). (a) depicts a sub-network of between-pathway interactions. Each node represents a pathway with the node size proportionate to its degree and each edge represents an inferred interaction. The inferred interactions in this community imply the comorbidity among infectious diseases, especially hepatitis B and C, and more than half of all cancer types in this study through the contribution of the inflammatory signaling pathways namely, NF- κ B and Fc ϵ RI. (b) illustrates the comorbidity of hepatitis B and thyroid cancer through the interactions of NF- κ B and Fc ϵ RI. Those mechanisms were previously confirmed by separated studies.^{30–33}

each pathway, called a gene–pathway matrix. The second matrix $\mathbf{S} \in \mathbb{R}^{P \times D}$ corresponds to the degree of pathway responsiveness to each condition, called a pathway-condition matrix. Note that P is the number of pathways shared by the matrix \mathbf{B} and the matrix \mathbf{S} , since pathways are regarded as the latent factors underlying both genes and conditions. Similar to FacPad,¹² we used the prior knowledge of gene–pathway memberships denoted by a matrix $\mathbf{K} \in \{0,1\}^{G \times P}$ from KEGG¹⁹ to force the sparsity (the pattern of 0's entries) of the matrix \mathbf{B} . We developed a GMRF model within the matrix decomposition with the aim of capturing pathway dependencies by imposing a Gaussian distribution on the matrix \mathbf{S} with a precision (inverse covariance) matrix $\Phi \in \mathbb{R}^{P \times P}$. Consequently, we drew the undirected links between any two pathways according to the non-zero off-diagonal elements of the matrix Φ . Meanwhile, we determined pathway responsive to each condition from the matrix \mathbf{S} .

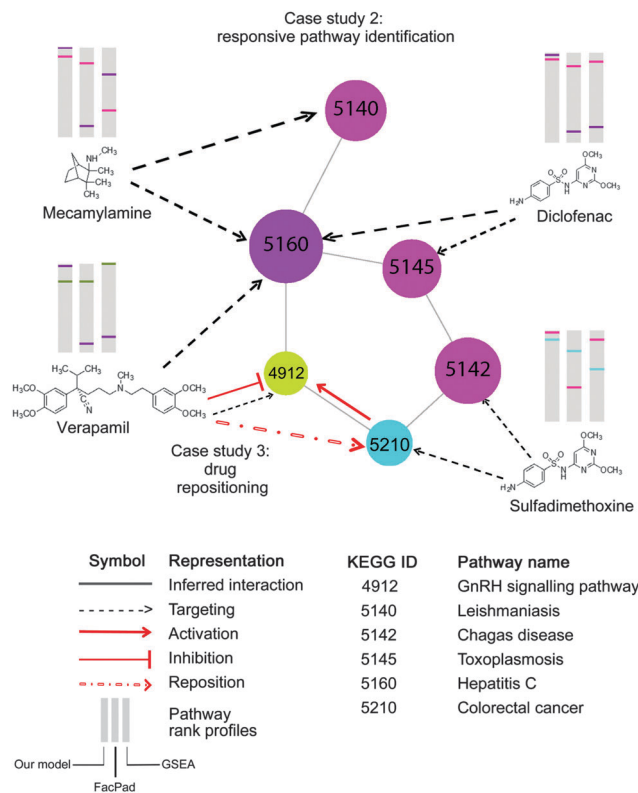


Fig. 8 Application of the inferred pathway network to enhance the identification of pathway responsiveness to drug treatments, (case study 2) and drug repositioning (case study 3). Each node represents a pathway with the corresponding KEGG ID. This part of the pathway network derived from Fig. 6b is targeted by four drugs, Mecamylamine, Verapamil, Diclofenac, and Sulfadimethoxine, as documented in CTD. In the diagram, there are three pathway rank profiles inferred by our model, FacPad, and GSEA are shown above each chemical structure. The position of any targeted pathway within each rank profile is represented by a line with the same colour as the corresponding targeted pathway. As seen on the pathway rank profiles inferred by our model, any two pathways that were closely correlated to each other were placed in the upper rank, unlike FacPad and GSEA. This proves that the inferred pathway interactions can help improve the model to identify pathway responsiveness to drug treatments. As seen in case study 3, the pathway network also enables drug repositioning; particularly a repositioning of Verapamil for recovering the colorectal cancer state.⁴¹ With the inferred pathway interlinks, we may make an assumption that the GnRH signaling pathway is the underlying mechanism for such repositioning, therefore, providing a bridge for Verapamil to counteract the effects of colorectal cancer. These findings are consistent with the studies claiming that GnRH hormone is activated by colorectal cancer,⁴⁰ but inhibited by Verapamil.⁵⁹

Fig. 9 shows our methodology in a schematic view. The following subsections are the brief introduction of GMRF, the mathematical description of our model in detail and our inference method.

4.3 Gaussian Markov Random Field (GMRF)

GMRF, referred to as a Gaussian Graphical model (GGM) interchangeably,⁴⁷ is a special case of Markov Random Field forming with respect to an undirected graph if it satisfies the Markov properties.⁴⁸ An N -dimensional random vector \mathbf{x} which



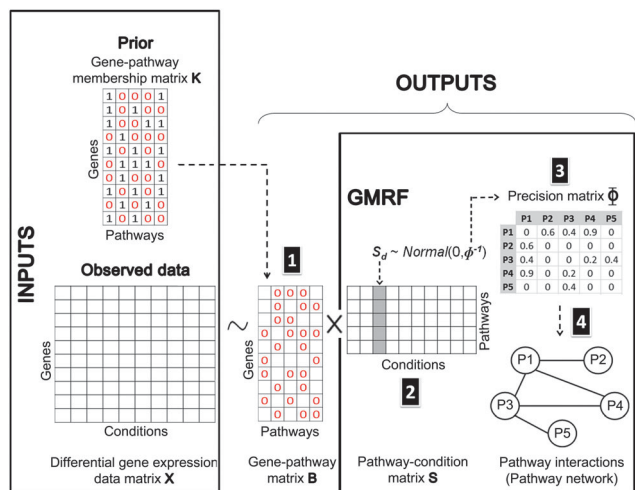


Fig. 9 Bayesian matrix factorisation modeling with GMRF. Our model requires two input types: an observed differential gene expression data matrix \mathbf{X} under conditions of interest and a pre-defined gene-pathway membership binary matrix \mathbf{K} . The main task is to decompose the matrix \mathbf{X} into a gene–pathway matrix \mathbf{B} and a condition–pathway matrix \mathbf{S} : $\mathbf{X} \sim \mathbf{B}\mathbf{S}$. The first step (1) is to make inference on the matrix \mathbf{B} . The matrix \mathbf{K} is used as prior knowledge to guide the sparsity pattern of the matrix \mathbf{B} .¹² The significant contribution to this work is the modeling of a Gaussian distribution with a zero mean and a precision Φ on the matrix \mathbf{S} . Thus, the next two steps (2 and 3) are to infer the matrix \mathbf{S} and its precision matrix Φ . The values in each column of the matrix \mathbf{S} can reflect the pathway responsiveness to the corresponding drug treatments or disease conditions. According to the concept of GMRF that an undirected graph is encoded by non-zero entries in the off-diagonal precision matrix, the values in the matrix Φ represent the conditional correlation of every pathway pair. In the last step (4), a pathway interaction network can be finally constructed, given the matrix Φ .

is defined by GMRF⁴ is assumed to follow a zero-mean multivariate Gaussian distribution with a precision matrix $\Phi = [[\Phi_{ij}]]$; $i, j \in \{1, \dots, N\}$ as shown in eqn (4):

$$P(\mathbf{x}) = (2\pi)^{-\frac{N}{2}} |\Phi|^{\frac{1}{2}} \exp\left(-\frac{1}{2} \mathbf{x}^T \Phi \mathbf{x}\right) \quad (4)$$

According to the definition of GMRF,⁴ the interpretation of the precision matrix is as follows. Zero elements in the off-diagonal matrix indicate the conditional independence. Non-zero off-diagonal entries in the precision matrix encode the undirected connections between the two corresponding random variables. The magnitude of the correlation for any two variables x_i and x_j ; $i, j \in \{1, \dots, N\}$ conditioned on the rest can be calculated in eqn (5):

$$\text{Corr}(x_i, x_j | x_{\setminus ij}) = \left| \frac{\phi_{ij}}{\sqrt{\phi_{ii}\phi_{jj}}} \right| \quad (5)$$

It is remarked that GMRF contains two desirable characteristics. Firstly, it can encode any arbitrary typologies. Secondly, it allows us to directly interpret the conditional independence from the precision matrix.

4.4 Model description

The observed differential gene expression data matrix $\mathbf{X} = [[x_{gd}]]$ was linearly decomposed into two matrices: a gene–pathway matrix $\mathbf{B} = [[b_{gp}]]$ and a pathway–condition matrix $\mathbf{S} = [[s_{pd}]]$,

where $g \in \{1, \dots, G\}$, $d \in \{1, \dots, D\}$, and $p \in \{1, \dots, P\}$. Such decomposition can be represented in an element-wise linear combination with an additive noise model as shown in eqn (6):

$$\mathbf{x}_{gd} = \sum_{p=1}^P b_{gp} s_{pd} + \varepsilon; \varepsilon \in \mathbb{R} = \text{random noise.} \quad (6)$$

Each variable was modeled as the following:

$$x_{gd} = \sum_{p=1}^P b_{gp} s_{pd} = \mathbf{b}_g \mathbf{s}_d + \varepsilon; \varepsilon \sim \text{Normal}(0, \tau_\varepsilon^{-1})$$

$$\tau_\varepsilon \sim \text{Gamma}(\alpha_\varepsilon, \beta_\varepsilon)$$

$$b_{gp} = \begin{cases} 0, & \text{if } k_{gp} = 0 \\ \text{Normal}(b_{gp} | 0, \tau_B^{-1}), & \text{if } k_{gp} = 1 \end{cases}$$

$$\tau_B \sim \text{Gamma}(\alpha_B, \beta_B)$$

$$\mathbf{s}_d \sim \text{GMRF}(\mathbf{0}, \Phi^{-1})$$

$$\Phi \sim \text{Wishart}(\nu, \Psi)$$

First of all, we modeled the noise ε with a zero-mean Gaussian with the precision τ_ε . We also put a conjugate prior Gamma distribution with the shape parameter α_ε and the rate parameter β_ε on τ_ε . This noise model was applied for every entry of the matrix \mathbf{X} , known as an isotopic Gaussian noise model.

Likewise, we put a zero-mean Gaussian distribution with the precision τ_B on every entry of the matrix \mathbf{B} . We also exploited the pre-defined gene–pathway memberships matrix $\mathbf{K} = [[k_{gp}]]$, where $k_{gp} = 1$ if gene g belonged to pathway p and $k_{gp} = 0$ otherwise, to control the sparsity pattern of the matrix \mathbf{B} .¹² Therefore, the values in the matrix \mathbf{B} suggested the strength of the gene membership in each pathway, which was not specified by the binary matrix \mathbf{K} .

In order to capture the relations of the latent pathways, we put the zero-mean GMRF with the precision matrix Φ on every condition vector of the matrix \mathbf{S} (eqn (4)). With the GMRF, the conditional correlations between any two pathways were described by the parameter $\Phi = [[\Phi_{ij}]]$; $i, j \in \{1, \dots, P\}$ (eqn (5)). We next constructed an undirected graph illustrating such relations. Let $G = (V, E)$ denotes an undirected graph where nodes represent hidden pathways and edges denote any pairwise relations. An edge between node i and j where $(i, j) \in V \times V$ is drawn if and only if $\phi_{ij} > 0$. The Wishart distribution, a conjugate prior of normal likelihood function, with the degree of freedom ν and the scale matrix Ψ was used as the prior of Φ .

4.5 Inference

According to the models described above, we needed to make inference on τ_ε , τ_B , \mathbf{B} , \mathbf{S} , and Φ with a setting of hyper-parameters (α_ε , β_ε , α_B , β_B , ν , and Ψ). However, only the matrix \mathbf{S} and the matrix Φ were our main interests for further analysis. Under a Bayesian framework, we developed the correlated pathways Gibbs sampling algorithm to approximate the joint distribution of those five parameters (Algorithm 1).



Algorithm 1: Correlated pathways Gibbs sampling

Inputs: differential gene expression data matrix \mathbf{X} and gene–pathway memberships matrix \mathbf{K}

Hyper-parameters: $\Omega = \{\alpha_\varepsilon, \beta_\varepsilon, \alpha_B, \beta_B, \nu, \Psi\}$

Results: samples from the joint posterior distribution

$$P(\tau_\varepsilon^{(t)}, \tau_B^{(t)}, \mathbf{B}^{(t)}, \Phi^{(t)}, \mathbf{S}^{(t)} | \mathbf{X}, \mathbf{K}, \Omega)$$

Initialization: $\{\tau_\varepsilon^{(0)}, \tau_B^{(0)}, \mathbf{B}^{(0)}, \Phi^{(0)}, \mathbf{S}^{(0)}\}$

begin

for each sampling iteration t do

Draw $\tau_\varepsilon^{(t)} \sim P(\tau_\varepsilon | \mathbf{X}, \mathbf{B}^{(t-1)}, \mathbf{S}^{(t-1)}, \alpha_\varepsilon, \beta_\varepsilon)$

Draw $\tau_B^{(t)} \sim P(\tau_B | \mathbf{B}^{(t-1)}, \alpha_B, \beta_B)$

for each element $g \in G$ do

Draw $b_g^{(t)} \sim P(b_g | \mathbf{X}, \mathbf{S}^{(t-1)}, \tau_\varepsilon^{(t)}, \tau_B^{(t)})$

end

Normalise such that $\sum_{p=1}^P b_{gp} = 1$

Draw $\Phi^{(t)} \sim P(\Phi | \mathbf{S}^{(t-1)}, \nu, \Psi)$

for each element $d \in D$ do

Draw $\mathbf{s}_d^{(t)} \sim P(\mathbf{s}_d | \mathbf{X}, \mathbf{B}^{(t)}, \tau_\varepsilon^{(t)}, \Phi^{(t)})$

end

end

end

Below is the conditional posterior distribution for each step in the correlated pathways Gibbs sampling. The first two (1–2) demonstrate those of the inverse variances in the noise model ε and the gene–pathway matrix \mathbf{B} respectively. The calculation in the third (3) is consistent to that of FacPad.¹² The last two (4–5) allow us to learn pathway responsiveness together with between-pathway interactions (see the ESI† for the calculation methods in detail):

$$(1) \tau_\varepsilon \sim P(\tau_\varepsilon | \mathbf{X}, \mathbf{B}, \mathbf{S}, \alpha_\varepsilon, \beta_\varepsilon)$$

$$\begin{aligned} &\propto \prod_{g=1}^G \prod_{d=1}^D \mathcal{N}(x_{gd} | \mathbf{b}_g \mathbf{s}_d, \tau_\varepsilon^{-1}) \Gamma(\tau_\varepsilon | \alpha_\varepsilon, \beta_\varepsilon) \\ &\propto \Gamma(\alpha_\varepsilon^*, \beta_\varepsilon^*) \end{aligned}$$

$$\alpha_\varepsilon^* = \alpha_\varepsilon + \frac{GD}{2} \text{ and } \beta_\varepsilon^* = \beta_\varepsilon + \frac{1}{2} \sum_{g=1}^G \sum_{d=1}^D (x_{gd} - \mathbf{b}_g \mathbf{s}_d)^2.$$

$$(2) \tau_B \sim P(\tau_B | \mathbf{B}, \alpha_B, \beta_B)$$

$$\begin{aligned} &\propto \prod_{(g,p) \in \mathcal{Z}} \mathcal{N}(b_{gp} | 0, \tau_B^{-1}) \cdot \Gamma(\tau_B | \alpha_B, \beta_B) \\ &\propto \Gamma(\alpha_B^*, \beta_B^*) \end{aligned}$$

$$\mathcal{Z} = \{(g,p) \in G \times P | k_{gp} = 1\}, \alpha_B^* = \alpha_B + \frac{|\mathcal{Z}|}{2},$$

$$\text{and } \beta_B^* = \beta_B + \frac{1}{2} \sum_{(g,p) \in \mathcal{Z}} b_{gp}^2.$$

$$(3) \mathbf{b}_g \sim P(\mathbf{b}_g | \mathbf{X}, \mathbf{S}, \tau_\varepsilon, \tau_B)$$

$$\propto \mathcal{N}(\mathbf{b}_g | \mu_B^*, (\Phi_B^*)^{-1}) \text{ if } k_{gp} = 1; p = 1, 2, 3, \dots, P$$

$\mu_B^* = (\Phi_B^*)^{-1}(\tau_\varepsilon \mathbf{S}^* \mathbf{x}_g^T)$, $\Phi_B^* = \tau_\varepsilon \mathbf{S}^* (\mathbf{S}^*)^T + \tau_B \mathbf{I}_{|\mathcal{S}^*|}$ and \mathbf{S}^* is the submatrix of \mathbf{S} with the row indices corresponding to the 1-entries of the vector \mathbf{k}_g .

$$(4) \Phi \sim P(\Phi | \mathbf{S}, \nu, \Psi)$$

$$\propto \prod_{d=1}^D \mathcal{N}(\mathbf{s}_d | \mathbf{0}, \Phi^{-1}) \cdot \mathcal{W}(\Phi | \nu, \Psi)$$

$$\propto \mathcal{W}(\Phi | \nu^*, \Psi^*)$$

$$\nu^* = \nu + D \text{ and } \Psi^* = \left(\Psi^{-1} + \sum_{d=1}^D (\mathbf{s}_d \mathbf{s}_d^T) \right)^{-1}.$$

$$(5) \mathbf{s}_d \sim P(\mathbf{s}_d | \mathbf{X}, \mathbf{B}, \tau_\varepsilon, \Phi)$$

$$\propto \mathcal{N}(\mathbf{x}_d | \mathbf{B} \mathbf{s}_d, \tau_\varepsilon^{-1} \mathbf{I}_G) \cdot \mathcal{N}(\mathbf{s}_d | \mathbf{0}, \Phi^{-1})$$

$$\propto \mathcal{N}(\mathbf{s}_d | \mu^*, (\Phi^*)^{-1})$$

$$\mu^* = (\Phi^*)^{-1}(\tau_\varepsilon \mathbf{B}^T \mathbf{x}_d) \text{ and } \Phi^* = \tau_\varepsilon \mathbf{B}^T \mathbf{B} + \Phi.$$

Our MATLAB implementation of the correlated pathway Gibbs sampling is available upon request to the corresponding author. The burn-in period can be selected according to the trace plots. Moreover, to decrease autocorrelation, samples from the Gibbs sampling can be collected subject to the thinning rate, and then be averaged across the collecting iterations to form the final estimations.

5 Conclusions

Given differential gene expression data of drug treatments and the prior knowledge of gene memberships in each pathway of interest, we have presented Bayesian factor modeling with GMRF to identify pathway responsiveness to drug treatments, concurrently with the reconstruction of between-pathway interactions.

Specifically, we treated all pathways as latent variables, of which gene members were pre-defined. We then applied a Bayesian matrix factorisation model to determine pathways that were perturbed specific to drug treatments.¹² The underlying assumption is that gene expression data arise from the effects of perturbed gene members of the pathways responsive to drug treatments.¹² Therefore, a gene expression data matrix was decomposed into a gene–pathway matrix indicating gene membership strength in each pathway and a drug–pathway matrix reflecting pathway responsiveness to each drug.

More importantly, we extended the Bayesian matrix factorisation models with a GMRF prior. This augmentation was inspired by the fact that genes could pass their signals across different groups or pathways.¹⁶ We imposed a Gaussian distribution with a zero mean and a precision matrix (an inverse covariance matrix) on the drug–pathway matrix. This precision matrix was mapped to an undirected graph depicting pairwise dependencies between pathways. Here, the interactions between any pair of pathways were drawn if and only if they were direct relationships without the mediation through any other pathway. We quantified the between-pathway interactions by calculating their correlations directly from the precision matrix under the GMRF framework. However, we can explore indirect relationships from the network of all direct interactions.



Our method can infer complex relations between two pathways through other layers of molecules such as proteins or metabolites, which cannot be observed by only overlapping perturbed genes. With our approach, the complexity can be simplified by the replacement of a link between pathways derived from the co-occurrence of pathways from the observed gene expression data.

The combination of the Bayesian factor model and the GMRF prior allows us to identify pathway responsiveness and to extract between-pathway interactions in a unified framework. As a result, our method yielded a higher average precision than the existing methods for identifying pathway responsiveness to drugs that affect multiple pathways. This contribution is advantageous to the analysis of disease gene expression data as the number of associated pathways is increasing in proportion to disease complexity, comorbidity,⁴⁹ and progression time.⁵⁰ In addition, the network of between-pathway interactions can also provide the mechanistic insights in terms of pathway-based functionality that accommodate the studies of disease comorbidity, drug repositioning, and tissue-specific comparative analysis.

Acknowledgements

We thank Dr Viet Anh Nguyen for a productive discussion on Bayesian approaches. We thank FP7-ICT Mission T2D for funding. NP acknowledges the Royal Thai Government Scholarship.

References

- 1 A. Subramanian, P. Tamayo, V. K. Mootha, S. Mukherjee, B. L. Ebert, M. A. Gillette, A. Paulovich, S. L. Pomeroy, T. R. Golub, E. S. Lander and J. P. Mesirov, *Proc. Natl. Acad. Sci. U. S. A.*, 2005, **102**, 15545–15550.
- 2 K.-I. Goh, M. E. Cusick, D. Valle, B. Childs, M. Vidal and A.-L. Barabási, *Proc. Natl. Acad. Sci. U. S. A.*, 2007, **104**, 8685–8690.
- 3 Z. Wu, Y. Wang and L. Chen, *Mol. BioSyst.*, 2013, **9**, 1268–1281.
- 4 H. Rue and L. Held, *Gaussian Markov Random Fields: Theory and Applications*, Chapman & Hall, London, 2005, vol. 104.
- 5 Y. C. MacNab, *Stat. Methods Med. Res.*, 2011, **20**, 49–68.
- 6 O. Demirkaya, M. H. Asyali and M. M. Shoukri, *Bioinformatics*, 2005, **21**, 2994–3000.
- 7 B. Peng, D. Zhu, B. P. Ander, X. Zhang, F. Xue, F. R. Sharp and X. Yang, *PLoS One*, 2013, **8**, e67672.
- 8 Z. Wei and H. Li, *Bioinformatics*, 2007, **23**, 1537–1544.
- 9 Y. Silberberg, A. Gottlieb, M. Kupiec, E. Ruppín and R. Sharan, *J. Comput. Biol.*, 2012, 163–174.
- 10 Y.-Q. Qiu, S. Zhang, X.-S. Zhang and L. Chen, *Syst. Biol.*, 2009, **3**, 475–486.
- 11 Y. Wang and Y. Xia, *Proc. Optim. Syst. Biol.*, 2008, **9**, 333–340.
- 12 H. Ma and H. Zhao, *Bioinformatics*, 2012, **28**, 2662–2670.
- 13 K. Kavukcuoglu, H. Park, Y. He and Y. Qi, *NIPS*, 2012, pp. 2375–2383.
- 14 J. D. Lafferty and D. M. Blei, *Advances in neural information processing systems*, 2005, pp. 147–154.
- 15 W. Luo, M. S. Friedman, K. D. Hankenson and P. J. Woolf, *BMC Syst. Biol.*, 2011, **5**, 82.
- 16 H. Pang and H. Zhao, *BMC Bioinf.*, 2008, **9**, 87.
- 17 J. Lamb, E. D. Crawford, D. Peck, J. W. Modell, I. C. Blat, M. J. Wrobel, J. Lerner, J.-P. Brunet, A. Subramanian, K. N. Ross, M. Reich, H. Hieronymus, G. Wei, S. A. Armstrong, S. J. Haggarty, P. A. Clemons, R. Wei, S. A. Carr, E. S. Lander and T. R. Golub, *Science*, 2006, **313**, 1929–1935.
- 18 J. Lamb, *Nat. Rev. Cancer*, 2007, **7**, 54–60.
- 19 M. Kanehisa, S. Goto, Y. Sato, M. Furumichi and M. Tanabe, *Nucleic Acids Res.*, 2012, D109–D114.
- 20 A. P. Davis, C. G. Murphy, R. Johnson, J. M. Lay, K. Lennon-Hopkins, C. Saraceni-Richards, D. Sciaky, B. L. King, M. C. Rosenstein, T. C. Wiegers and C. J. Mattingly, *Nucleic Acids Res.*, 2013, **41**, D1104–D1114.
- 21 R. Baeza-Yates and B. Ribeiro-Neto, *Modern information retrieval*, Addison Wesley, England, 1999.
- 22 K. Järvelin and J. Kekäläinen, *ACM Trans. Inf. Syst.*, 2002, **20**, 422–446.
- 23 C. V. Dang, *Genes Dev.*, 2012, **26**, 877–890.
- 24 C. de Martel, J. Ferlay, S. Franceschi, J. Vignat, F. Bray, D. Forman and M. Plummer, *Lancet Oncol.*, 2012, **13**, 607–615.
- 25 J. Parsonnet, *Environ. Health Perspect.*, 1995, **103**, 263.
- 26 V. Samaras, P. I. Rafailidis, E. G. Mourtzoukou, G. Peppas and M. E. Falagas, *J. Infect. Dev. Countries*, 2010, **4**, 267–281.
- 27 Q. Wang, W. Liu, S. Ning, J. Ye, T. Huang, Y. Li, P. Wang, H. Shi and X. Li, *Eur. J. Hum. Genet.*, 2012, **20**, 1162–1167.
- 28 D.-S. Lee, J. Park, K. A. Kay, N. A. Christakis, Z. N. Oltvai and A.-L. Barabási, *Proc. Natl. Acad. Sci. U. S. A.*, 2008, **105**, 9880–9885.
- 29 Y. Li and P. Agarwal, *PLoS One*, 2009, **4**, e4346.
- 30 D. Gutierrez, P. Guardia, J. Delgado, J. Gutiérrez, F. Monteseirin, A. De la Calle, P. Lobatón, A. Senra and J. Conde, *J. Invest. Allergol. Clin. Immunol.*, 1997, **7**, 119.
- 31 S. Klemm and J. Ruland, *Immunobiology*, 2006, **211**, 815–820.
- 32 I. Palona, H. Namba, N. Mitsutake, D. Starenki, A. Podtcheko, I. Sedliarou, A. Ohtsuru, V. Saenko, Y. Nagayama and K. Umezawa, *et al.*, *Endocrinology*, 2006, **147**, 5699–5707.
- 33 Y. Kato, H. Ying, L. Zhao, F. Furuya, O. Araki, M. Willingham and S. Cheng, *Oncogene*, 2005, **25**, 2736–2747.
- 34 A. Antonelli, C. Ferri, P. Fallahi, A. Pampana, S. M. Ferrari, L. Barani, S. Marchi and E. Ferrannini, *Thyroid*, 2007, **17**, 447–451.
- 35 F. Al-Mulla, M. S. Bitar, M. Al-Maghrebi, A. I. Behbehani, W. Al-Ali, O. Rath, B. Doyle, K. Y. Tan, A. Pitt and W. Kolch, *Cancer Res.*, 2011, **71**, 1334–1343.
- 36 K. Meyer, M. Ait-Goughoulte, Z.-Y. Keck, S. Fong and R. Ray, *J. Virol.*, 2008, **82**, 2140–2149.
- 37 A. Gottlieb, G. Y. Stein, E. Ruppín and R. Sharan, *Mol. Syst. Biol.*, 2011, **7**, 496.
- 38 F. Napolitano, Y. Zhao, V. M. Moreira, R. Tagliaferri, J. Kere, M. D'Amato and D. Greco, *J. Cheminf.*, 2013, **5**, 30.
- 39 K. Yu, P. Rosenblum and R. Peter, *Gen. Comp. Endocrinol.*, 1991, **81**, 256–267.
- 40 J. Engel, G. Emons, J. Pinski and A. V. Schally, *Expert Opin. Invest. Drugs*, 2012, **21**, 891–899.
- 41 Y. Liu, Z. Lu, P. Fan, Q. Duan, Y. Li, S. Tong, B. Hu, R. Lv, L. Hu and J. Zhuang, *Cell Biochem. Biophys.*, 2011, **61**, 393–398.



- 42 D. Von Bubnoff, N. Novak, S. Kraft and T. Bieber, *Clin. Exp. Dermatol.*, 2003, **28**, 184–187.
- 43 B. Rayet and C. Gelinas, *Oncogene*, 1999, **18**, 6938–6947.
- 44 H. Wang, D. Rothenbacher, M. Löw, C. Stegmaier, H. Brenner and T. L. Diepgen, *Int. J. Cancer*, 2006, **119**, 695–701.
- 45 P. Oh, Y. Li, J. Yu, E. Durr, K. M. Krasinska, L. A. Carver, J. E. Testa and J. E. Schnitzer, *Nature*, 2004, **429**, 629–635.
- 46 J. E. Schnitzer, *Adv. Drug Delivery Rev.*, 2001, **49**, 265–280.
- 47 S. L. Lauritzen, *Graphical models*, Oxford University Press, Oxford, 1996, vol. 17.
- 48 D. Barber, *Bayesian Reasoning and Machine Learning*, Cambridge University Press, Cambridge, 2012.
- 49 E. Capobianco and P. Lio, *Trends Mol. Med.*, 2013, **19**, 515–521.
- 50 L. Hood, *Rambam Maimonides Med. J.*, 2013, **4**, e0012.

